The
University
Of
Sheffield.

This is a repository copy of *High frequency voltage injection based stator inter-turn fault detection in permanent magnet machines*.

White Rose Research Online URL for this paper:
https://eprints.whiterose.ac.uk/163385/

Version: Accepted Version

White Rose
university consortium
Universities of Leeds, Sheffield & York

eprints@whiterose.ac.uk
https://eprints.whiterose.ac.uk/

High Frequency Voltage Injection Based Stator Inter-Turn Fault Detection in Permanent Magnet Machines

Rongguang Hu, *Student Member, IEEE*, Jiabin Wang, *Senior Member, IEEE*, Andrew R Mills, Ellis Chong, Zhigang Sun

Abstract- An inter-turn short-circuit fault in the stator winding of an electric machine, denoted as turn fault, has been recognized as one of the most severe faults in permanent magnet machines which requires swift and reliable detection, in order to implement appropriate mitigations. The asymmetry brought by a turn fault is widely used for the fault detection. However, similar features also emerges in a less severe high resistance connection (HRC) fault, which may led to incorrect fault identification. In this paper, a more exclusive turn fault detection method with the ability to differentiate from the HRC fault is proposed. It injects high frequency square wave voltage signals and makes use of the difference in high frequency impedance under the two fault conditions. The sensitivity to HRC fault is largely reduced. The proposed turn fault indicator is independent of operating conditions and robust with respect to state transients. This method is validated in a fault tolerant permanent magnet assisted synchronous reluctance machine drive.

Index Terms—Permanent magnet machines, inter-turn fault, high resistance connection fault, fault detection, high frequency voltage injection

I. INTRODUCTION

Stator related faults have been reported as the common faults in electrical machines, which can account for 21%-37% of the total machine failures, according to the industrial surveys in [1]. Therefore, the diagnostics of these faults and the health monitoring are essential for the reliable and safe operation. Two types of the stator faults, i.e. inter-turn short circuit faults and the high resistance connection (HRC) faults, have been investigated widely for their diagnostic and mitigation, to prevent further damages and facilitate fault-tolerant operations.

Inter-turn faults or turn faults are caused by insulation failures but may develop into more serious inter-phase or phase-to-ground faults very quickly if no preventive measures are taken [2]. Insulation failures are attributed to excessive temperature, voltage stresses, vibration, and aging. The large circulating current generated in the short-circuited paths may demagnetize the magnets irreversibly [3], and degrade the performance. More seriously, it may cause a rapid increase in the temperature which accelerates the insulation deterioration process. The damage to the machine can be quick and catastrophic. Thus, prompt and reliable diagnostic algorithms are essential, and have been extensively studied.

Among all the existing turn fault detection techniques, quite a few of them are based on detection of the asymmetry introduced by turn fault in a three phase balanced system. The detection of the 2nd harmonic in dq currents and voltages are

proposed in [4][5]. Other methods based on the 2nd harmonic of power [6], and the park's vector [7] can be seen as the extensions but with the same principle. Similarly, the negative sequence components are also the results of the broken symmetry when a turn fault occurs, which have been pointed out in [2] that they are equivalent to the detection technique based on the 2nd harmonic. Therefore, the detection based on the negative sequence currents and voltages are also widely researched [8][9]. However, the effectiveness could be affected by the bandwidth of the current regulators in a closed-loop controlled drive. Other popular techniques are based on the zero sequence voltage [10] or current [11], which detect their fundamental component as the signature of the asymmetry in turn fault conditions. They improve the detection sensitivity and accuracy, but require an access to the neutral point of the stator windings as well as an extra voltage sensor.

An HRC fault can be caused by loose connection in any device between the inverter and the machine or damaged connectors and solder points. Also, due to oxidization, the real connections are only established where the non-conductive oxide film is fractured by the contact pressure. Consequently, with this cluster of micro-spots as the conducting part, the possibility of high resistance connection is increased [12][13]. This type of fault can cause local over-heating on the contact surface and subsequently damage the connection [14]. The damage to the machine itself, however, is limited, which is different from that caused by a turn fault. In most cases, an HRC fault only deteriorates the operating performance of the machine, such as increase in torque ripple and reduction in efficiency. The less severe consequences require no urgent measures. Therefore, it is undesirable that a turn fault is misdiagnosed as an HRC fault, leading to inappropriate mitigation measures.

However, since the HRC fault also introduce asymmetry at the fundamental operating frequency, all the turn fault detection methods described above will be sensitive to an HRC fault, especially at low speed with high current, where the resistive voltage drop accounts more in the applied voltage. As a result, the risk of misdiagnosis increases. The detection and classification of these faults based on the zero sequence voltage and negative sequence current in an induction machine is investigated in [15], where both the amplitude and phase angle of the signals are obtained and compared according to different patterns for the two fault types. However, it is very sensitive to the machine parameters

which may vary in operations. In addition, the technique is only valid in steady-state conditions, and the feasibility in detecting faults during transient states remains a problem. In [16], the phase angle of both fundamental current and impedance are used to realize the fault classification. But the impedance phase angle obtained by prior measurement may change under different operating conditions.

Since the priority for the reliable detection of a turn fault is higher than an HRC fault, a more exclusive turn fault detection method which can discriminate an HRC fault is essential. Since the impact of the two fault types on the high frequency impedance is different, the detection methods based on high frequency signals possess more potential. The PWM ripple current based turn fault detection is proposed in [17] which utilizes the inherent high frequency switching harmonics. However, the symmetry of the high frequency voltages are still affected by the voltages at the fundamental frequency through change in modulation index in a fault condition in a closed-loop controlled drive. Thus, the effect of an HRC cannot be eliminated entirely. The extra high frequency signal injection is implemented for turn fault detection in induction machines in [18], where the dc components of the negative sequence high frequency currents are utilized. It can reduce the influence of the current regulator and working conditions, but the performance at transient states and the capability of differentiating from the HRC fault have not been discussed yet. These issues are explicitly addressed in the technique in [19]. However, the fact that it needs additional hardware and the access of phase neutral point could increase the cost and limit its application.

In this paper, a turn fault detection method based on injecting high frequency rotating square waveform voltages is proposed.

The characteristic features of the two fault conditions are firstly analyzed, and the difference of the fault impacts in high frequency domain is utilized for turn fault detection. The three corresponding high frequency currents are extracted by digital bandpass filters, and their RMS values are utilized to define a fault indicator presenting the overall asymmetry. It is shown that the proposed turn fault detection technique is insensitive to an HRC fault, independent of the operating conditions, and robust to transient states. The method is tested and validated on a fault tolerant permanent magnet assisted synchronous reluctance machine drive.

II. GOVERNING EQUATIONS IN FAULT CONDITIONS

To understand the difference in fault signatures between a turn fault and an HRC fault, the governing equations under the two fault conditions are derived based on the classical interior PM machine model, and the characteristic features of the two faults are analyzed.

A. Turn Fault

A turn fault occurs when different turns of the same coil begin to contact each other due to insulation breakdown. If the insulation degradation is severe, the contact resistance can be very low, creating a short-circuit path. Without loss of generality, the turn fault is assumed to be in phase A, whose winding is divided into healthy and faulted parts, as shown Fig. 1. The contact resistance is denoted as R_f. The ratio of the number of the short-circuited turns over the total number of the series turns in one phase is defined as μ, which represents the fault range between 0 and 1. The self-inductances of the healthy and faulted parts, and the mutual inductance between them are also defined. Since the back electromotive force (EMF) can be considered proportional to the number of turns, the EMFs in healthy and faulted parts can be calculated accordingly.

Based on the equivalent circuit, the model for fault conditions can be expressed in (1), where u_{ah} and u_{af} denote the voltages in the healthy and faulted parts of phase A winding respectively, i_f denotes the fault current caused by the short circuit, and λ_a , λ_b , and λ_c are the permanent magnet (PM) flux linkage in phases A, B, and C, respectively.
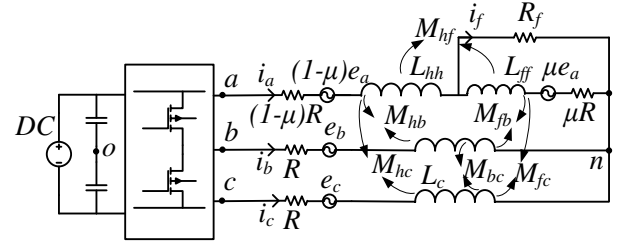

Fig. 1. Equivalent circuit and parameters in turn fault condition

$$\begin{cases} u_{ah} = (1-\mu)Ri_a + \dfrac{d\left[L_{hh}i_a + M_{hf}(i_a - i_f) + M_{hb}i_b + M_{hc}i_c + (1-\mu)\lambda_a \right]}{dt} \\ u_{af} = \mu R(i_a - i_f) + \dfrac{d\left[M_{hf}i_a + L_{ff}(i_a - i_f) + M_{fb}i_b + M_{fc}i_c + \mu\lambda_a \right]}{dt} \\ u_{bn} = Ri_b + \dfrac{d\left[M_{hb}i_a + M_{fb}(i_a - i_f) + L_b i_b + M_{bc}i_c + \lambda_b \right]}{dt} \\ u_{cn} = Ri_c + \dfrac{d\left[M_{hc}i_a + M_{fc}(i_a - i_f) + M_{cb}i_b + L_c i_c + \lambda_c \right]}{dt} \end{cases}$$

(1)

where R, L and M are the phase resistance, self- and mutual inductances as defined in Fig. 1.

According to [20] and [21], the following relationship between the self and mutual inductances related with the faulted turns can be obtained, shown in (2).

$$\begin{cases} L_{hh} + 2M_{hf} + L_{ff} = L_a \\ M_{hb} + M_{fb} = M_{ab} \\ M_{hc} + M_{fc} = M_{ac} \\ M_{hf} + L_{ff} = \mu L_a \\ M_{fb} = \mu M_{ab} \\ M_{fc} = \mu M_{ac} \end{cases}$$

(2)

Rearrange the phase voltage equations by applying $u_{an}=u_{ah}+u_{af}$ the three phase voltage equations in turn fault conditions can be derived as (3).

It can be seen from (3) that the turn fault affects both the resistive and inductive terms of the phase voltages. The voltage equation of the faulted part can be expressed as (4). For a given number of short-circuited turns, the lower R_f is, the larger i_f can reach, and the worse the scenario can be. Thus to evaluate the most severe condition and for the sake of simplicity, R_f is assumed zero in the subsequent analysis.

$$\begin{cases} u_{an} = Ri_a + e_a - \mu R i_f \\ \qquad + \dfrac{d(L_a i_a)}{dt} + \dfrac{d(M_{ab} i_b)}{dt} + \dfrac{d(M_{ac} i_c)}{dt} - \mu \dfrac{d(L_a i_f)}{dt} \\ u_{bn} = Ri_b + e_b \\ \qquad + \dfrac{d(L_b i_b)}{dt} + \dfrac{d(M_{ab} i_a)}{dt} + \dfrac{d(M_{bc} i_c)}{dt} - \mu \dfrac{d(M_{ab} i_f)}{dt} \\ u_{cn} = Ri_c + e_c \\ \qquad + \dfrac{d(L_c i_c)}{dt} + \dfrac{d(M_{ac} i_a)}{dt} + \dfrac{d(M_{bc} i_b)}{dt} - \mu \dfrac{d(M_{ac} i_f)}{dt} \end{cases} \quad (3)$$

$$\begin{aligned} u_f &= \mu R(i_a - i_f) + \mu \frac{d(L_a i_a + M_{ab} i_b + M_{ac} L_c)}{dt} - \frac{d(L_{ff} i_f)}{dt} + \mu e_a \\ &= R_f i_f \end{aligned} \quad (4)$$

When the three phase voltage equations are transformed to the rotating dq frame, the dq voltages are expressed in (5), where θ_e is the electrical angle, ω_e is the electrical angular speed, λ_{pm} is the permanent magnet flux linkage.

$$\begin{cases} u_d = R\,i_d + L_d \dfrac{di_d}{dt} - \omega_e L_q i_q + \dfrac{2}{3}\mu\omega_e L_d i_f \sin\theta_e \\ \qquad - \dfrac{2}{3}\mu\omega_e L_d \cos\theta_e \dfrac{di_f}{dt} - \dfrac{2}{3}\mu\omega_e L_q i_f \sin\theta_e - \dfrac{2}{3}\mu R i_f \cos\theta_e \\ u_q = R\,i_q + L_q \dfrac{di_q}{dt} + \omega_e(L_d i_d + \lambda_{pm}) + \dfrac{2}{3}\mu\omega_e L_q i_f \cos\theta_e \\ \qquad + \dfrac{2}{3}\mu\omega_e L_q \sin\theta_e \dfrac{di_f}{dt} - \dfrac{2}{3}\mu\omega_e L_d i_f \sin\theta_e + \dfrac{2}{3}\mu R i_f \cos\theta_e \end{cases} \quad (5)$$

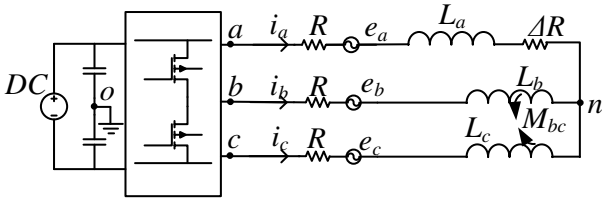*B. High Resistance Connection (HRC) Fault*

Fig. 2. Equivalent circuit in HRC fault condition and the measurement of zero sequence voltage

In an HRC fault condition, the machine windings can be represented with an additional resistor ΔR connected to the faulted phase winding, as shown in Fig. 2, assuming the fault occurs in phase A. The three phase voltage equations and the dq axis voltage equations in the HRC condition can be expressed in (6) and (7) respectively. It is evident that an HRC fault only influences the resistive term of the phase voltage.

$$\begin{cases} u_{an} = (R + \Delta R)i_a + \dfrac{d(L_a i_a)}{dt} + \dfrac{d(M_{ab} i_b)}{dt} + \dfrac{d(M_{ac} i_c)}{dt} + e_a \\ u_{bn} = Ri_b + \dfrac{d(L_b i_b)}{dt} + \dfrac{d(M_{ab} i_a)}{dt} + \dfrac{d(M_{bc} i_c)}{dt} + e_b \\ u_{cn} = Ri_c + \dfrac{d(L_c i_c)}{dt} + \dfrac{d(M_{ac} i_a)}{dt} + \dfrac{d(M_{bc} i_b)}{dt} + e_c \end{cases} \quad (6)$$

$$\begin{cases} u_d = R\,i_d + L_d \dfrac{di_d}{dt} - \omega_e L_q i_q + \dfrac{2}{3}\Delta R i_a \cos\theta_e \\ u_q = R\,i_q + L_q \dfrac{di_q}{dt} + \omega_e(L_d i_d + \lambda_{pm}) - \dfrac{2}{3}\Delta R i_a \sin\theta_e \end{cases} \quad (7)$$

III. HIGH FREQUENCY SIGNAL INJECTION

The detection of turn fault in the PM machine by using the inherent PWM switching high frequency components have been studied in [22] and [17]. However, when an HRC fault occurs, the 2nd harmonic in the dq command voltages caused by the asymmetry will lead to the asymmetrical reference voltages for PWM operations. Thus, the three phase high frequency components of the PWM voltages and the resultant high frequency currents become asymmetrical under an HRC fault, generating the similar fault signatures to those in turn fault conditions. This phenomenon is more apparent at lower speed where the effect of unbalanced resistive voltages on asymmetry is significant. At high speed, however, due to the large proportion of balanced back EMF and inductive voltage, the influence is weak, and the symmetry of the voltages can be preserved, making the PWM ripple current methods in [17] and [22] quite reliable for turn fault detection. Thus, the robustness of the turn fault detection against the HRC fault should be focused at low speed.

By comparing the voltage equations in (3) and (6), it is clear that the turn fault alters both the resistance and inductance, while the HRC fault only alters the resistance. Thus, a large difference between these two faults can be found in the high frequency impedance where the inductance is more dominant. If constant symmetric three high frequency voltages are imposed on the 3-phase windings, then the difference in the high frequency impedance can be captured in the corresponding high frequency currents, which can be used for the effective discrimination of the two fault types. In order to realise this, and to apply the similar comparative study of the high frequency currents in [22], a rotating square wave high frequency voltage injection is implemented.
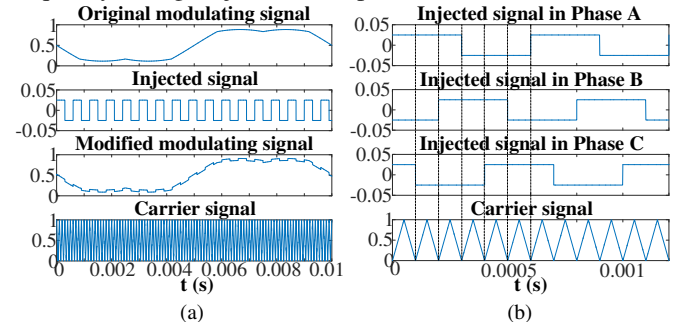

Fig. 3. (a) Modified SVPWM modulating signal with square wave signal injection. (b) Three phase injected square wave signals and the carrier signal

The rotating square waves for three phases should have 3-phase symmetry with 120 degree phase shift, thus only six states need to be produced, i.e. 101, 100, 110, 010, 011, 001, where 0 and 1 represent the lower and upper level of the square wave for each phase. The magnitude of the square wave is set to be 0.05 with respect to the normalised modulation index, and they are to be injected to the original modulating signals shown in Fig. 3(a) under the space vector PWM control strategy. In practice, the current sampling and modulation index updating frequency is equal to the switching frequency, 10 kHz used in this study. Thus, the injected square waveforms and their six states with respect to the carrier signal are shown in Fig. 3(b) at the highest possible frequency, being 1/6 of the carrier frequency. The modified modulating signals are compared with the triangular wave carrier signal to generate the gate signals for the inverter switches. The complete signal injection process is illustrated in Fig. 4. The original modulating signals generate the required three phase driving voltages which contains the fundamental component as well as the switching harmonics and their sidebands. The injected square wave voltages generate the three phase high frequency currents, which can be separated from both the fundamental and switching frequency components.
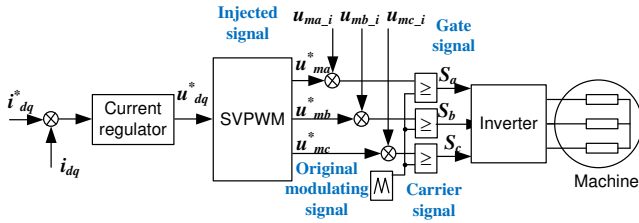

Fig. 4. Square wave signal injection implementation with current control

Since the neutral point of the 3-phase winding is floating, the zero sequence voltages, which consists of the 3rd and its integer multiple harmonics of the injected signal, are eliminated naturally in the phase voltages. The spectrum of the phase voltages are illustrated in Fig. 5. It is seen that the injected signal is at 1666.7 Hz which is 1/6 of the switching frequency of 10 kHz. Also, it has a good separation from both the fundamental frequency component and the switching sideband harmonics. Thus, a band pass filter (BPF) can be applied to acquire the interested frequency components.
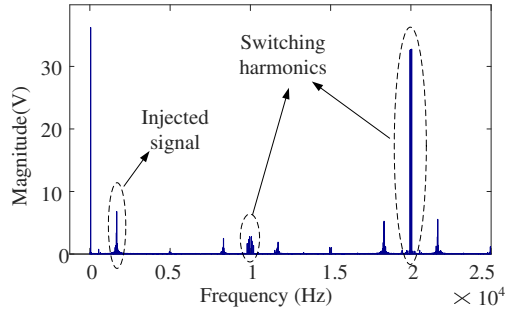

Fig. 5. (a).The equivalent injected signal referred to the winding neutral point, and (b) the spectrum of phase voltage

IV. FAULT FEATURE AT HIGH FREQUENCY

The benefit of the signal injection is that the high frequency voltages can be applied independently from the fundamental frequency voltages for machine operations. Thus, even in the fault conditions when the symmetry of the fundamental frequency voltages are broken, resulting in asymmetric SVPWM reference signals, the injected voltages are till symmetrical. Considering the dominant frequency component at the injected frequency, the injected phase voltages can be expressed as (8), where U_i and ω_i represent its amplitude and frequency.

$$\begin{cases} u_{am\_i} = U_i \sin \omega_i t \\ u_{bm\_i} = U_i \sin(\omega_i t - 2\pi/3) \\ u_{cm\_i} = U_i \sin(\omega_i t - 4\pi/3) \end{cases} \tag{8}$$

To analyse the three phase current signals in the IPM machine with saliency, the voltages are transformed into the rotating dq frame shown in (9) and applied to the voltage equations in the healthy condition given in (10). At the injected high frequency, the resistive voltage drop and the motional EMF can be neglected, compared to the transformer EMF, because ω_e is much smaller than ω_i. The current components can be expressed as (11). Thereafter, the currents components are transformed back into the abc frame given in (12) which can be measured and compared directly in practice.

$$\begin{cases} u_{d\_i} = U_i \sin(\omega_i t - \omega_e t) \\ u_{q\_i} = -U_i \cos(\omega_i t - \omega_e t) \end{cases} \tag{9}$$

$$\begin{cases} u_d = R\, i_d + L_d \dfrac{di_d}{dt} - \omega_e L_q i_q \\ u_d = R\, i_d + L_q \dfrac{di_d}{dt} + \omega_e (L_d i_d + \lambda_{pm}) \end{cases} \tag{10}$$

$$\begin{cases} i_{d\_i} \approx \dfrac{u_{d\_i}}{j(\omega_i - \omega_e)L_d} \\ i_{q\_i} \approx \dfrac{u_{q\_i}}{j(\omega_i - \omega_e)L_q} \end{cases} \tag{11}$$

$$\begin{cases} i_{a\_i} = -\dfrac{U_i}{\omega_i - \omega_e} \left[\begin{array}{l} \left(\dfrac{1}{2L_d} + \dfrac{1}{2L_q}\right)\cos \omega_i t \\ + \left(\dfrac{1}{2L_d} - \dfrac{1}{2L_q}\right)\cos\left[(\omega_i - 2\omega_e)t\right] \end{array} \right] \\[24pt] i_{b\_i} = -\dfrac{U_i}{\omega_i - \omega_e} \left[\begin{array}{l} \left(\dfrac{1}{2L_d} + \dfrac{1}{2L_q}\right)\cos(\omega_i t - \dfrac{2\pi}{3}) \\ + \left(\dfrac{1}{2L_d} - \dfrac{1}{2L_q}\right)\cos\left[(\omega_i - 2\omega_e)t + \dfrac{2\pi}{3}\right] \end{array} \right] \\[24pt] i_{c\_i} = -\dfrac{U_i}{\omega_i - \omega_e} \left[\begin{array}{l} \left(\dfrac{1}{2L_d} + \dfrac{1}{2L_q}\right)\cos(\omega_i t - \dfrac{4\pi}{3}) \\ + \left(\dfrac{1}{2L_d} - \dfrac{1}{2L_q}\right)\cos\left[(\omega_i - 2\omega_e)t + \dfrac{4\pi}{3}\right] \end{array} \right] \end{cases} \tag{12}$$

It should be noted that (12) also applies to HRC fault conditions, because the injected voltages remain symmetric and always satisfy (8), and the relevant terms in (7) are also negligible. Hence, the corresponding current components should be the same as that in the healthy conditions. It is clear that the current components at the injected frequency are symmetrical with identical amplitude and 120 degree phase difference among each other.

When a turn fault occurs in phase A, the dq axis voltage equations are expressed in (5). As the fault current also contains the injected frequency component, only the differential items are kept when rewriting the voltage equations at that frequency, shown in (13). The current components in the dq frames are solved in (14) and transformed back into the abc frame in (15). In addition to the symmetrical components shown in (12), the results also contain extra terms related to the fault current. It is evident that these extra terms are not symmetrical, so as the current components at the injected frequency in a turn fault condition. Therefore, only by examining the three phase currents at the injected frequency, the turn fault can be exclusively detected.

It should be pointed out that the effectiveness of the method is limited by the fundamental frequency. For the IPM machine under study, the fundamental frequency at the maximum speed of 19000 r/min is 950Hz, close to the injected frequency of 1.67 kHz. But as has been explained, this exclusive detection of turn fault is only required at low speed, typically below 1000 r/min. Thus, the feasibility of the high frequency injection can be guaranteed.

The above analysis is based on an IPM machine, but the conclusions also apply to an SPM machine, where there is no saliency and L_d equals to L_q. For the SPM machine, equation (12) can be simplified but equation (15) is still valid, thus the respective features of symmetry and asymmetry of high frequency currents in healthy and turn fault conditions remain the same.

$$\begin{cases} u_{d\_i} = j(\omega_i - \omega_e)i_{d\_i}^{TF}L_d - \dfrac{2}{3}j(\omega_i - \omega_e)\mu\omega_e L_d \cos\theta_e i_{f\_i} \\ u_{q\_i} = j(\omega_i - \omega_e)i_{q\_i}^{TF}L_q + \dfrac{2}{3}j(\omega_i - \omega_e)\mu\omega_e L_q \sin\theta_e i_{f\_i} \end{cases} \quad (13)$$

$$\begin{cases} i_{d\_i}^{TF} = i_{d\_i} + \dfrac{2}{3}\mu\omega_e \cos\theta_e i_{f\_i} \\ i_{q\_i}^{TF} = i_{q\_i} - \dfrac{2}{3}\mu\omega_e \sin\theta_e i_{f\_i} \end{cases} \quad (14)$$

$$\begin{cases} i_{a\_i}^{TF} = i_{a\_i} + \dfrac{2}{3}\mu\omega_e i_{f\_i} \\ i_{b\_i}^{TF} = i_{b\_i} - \dfrac{1}{3}\mu\omega_e i_{f\_i} \\ i_{c\_i}^{TF} = i_{c\_i} - \dfrac{1}{3}\mu\omega_e i_{f\_i} \end{cases} \quad (15)$$

V. DIGITAL SIGNAL PROCESSING

The signal processing steps to obtain the fault indicator is similar to that in [17]. The high frequency currents need to be filtered and their RMS value is obtained to represent the significance. The ratios of the RMS values among three phases are calculated to indicate the asymmetry change, and then the standard deviation of the ratios is calculated as the fault indicator.

Since the injected frequency is 1/6 of the sampling frequency of 10 kHz, the resultant frequency components can be extracted by a digital BPF. Considering the processing power in the micro controller, a digital infinite impulse response (IIR) filter is designed with the transfer function given in (16), where z denotes the Z transformation operator. The coefficients are calculated to yield the centre frequency at 1667Hz with a bandwidth 167Hz. The Bode plot of the filter is shown in Fig. 6.

The three identical digital filters are implemented for the three phase currents simultaneously, after which their RMS values are calculated separately according to (17). The interval of such discrete calculation is set to one electrical cycle, in order to minimize the ripples on the results and achieve a quicker response. The whole signal processing is executed in the DSP controller, thus there is no need of additional hardware, as long as current transducers are available.

$$\frac{Y(z)}{X(z)} = \frac{b(1) + b(2)z^{-1} + b(3)z^{-2} + b(4)z^{-3} + b(5)z^{-4}}{a(1) + a(2)z^{-1} + a(3)z^{-2} + a(4)z^{-3} + a(5)z^{-4}} \quad (16)$$

where X denotes the input, and Y denotes the output of the digital IIR filter.
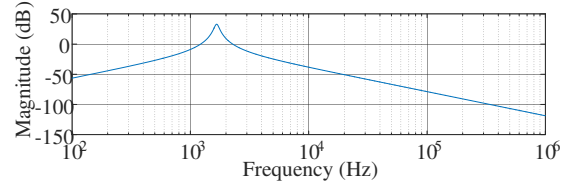

Fig. 6. The Bode plot of the digital bandpass filter

$$\begin{aligned} RMS(n) &= \sqrt{\sum_{i=n-T_e}^{n}\left[y(i)\cdot y(i)\right]} \\ T_e &= \left\lfloor \frac{2\pi}{\omega_e} \right\rfloor \end{aligned} \quad (17)$$

The ratios of the RMS currents among all three phases can be evaluated in (18). These ratios are a constant of 1 in healthy and HRC fault conditions. Only under turn fault conditions, the ratios deviate from 1. To obtain an overall signature of the broken symmetry, the fault indicator is defined as the standard deviation of the three ratios, given in (19). The abnormal changes in all three phase high frequency currents due to turn faults are captured, thus enhancing the detection effectiveness.

$$k_{ab} = \frac{i_{a\_rms}}{i_{b\_rms}}, k_{bc} = \frac{i_{b\_rms}}{i_{c\_rms}}, k_{ca} = \frac{i_{c\_rms}}{i_{a\_rms}} \quad (18)$$

$$k_{ave} = \frac{k_{ab} + k_{bc} + k_{ca}}{3}$$

$$SD = \sqrt{\frac{\left(k_{ab} - k_{ave}\right)^2 + \left(k_{bc} - k_{ave}\right)^2 + \left(k_{ca} - k_{ave}\right)^2}{3}} \quad (19)$$

VI. EXPERIMENTAL RESULTS

A fault tolerant machine drive based on permanent magnet assisted synchronous reluctance machine (PMA SynRM) reported in [23] is used for the validation of the proposed fault detection method. It has 36 slots and 3 pole pairs, with three independent 3-phase windings, which are segregated into triple redundant 3-phase winding configuration, as shown in Fig. 7. Since there is no overlap between two different 3-phase winding sets, the risk of a short circuit in two 3-phase sets is largely reduced. Also, the degradation or failure on one 3-phase winding set and the heat generated by the fault are not likely to transmit to the windings of the other 3-phase sets. Each 3-phase winding set ABC, DEF, GHI forms a balanced 3-phase system in space and time, and is controlled independently by three separate 3-phase inverters in the same way as a 3-phase IPM machine. Such physical, thermal and electrical isolation guarantees the fault tolerant capability when a fault occurs in one 3-phase winding set and a mitigation action is taken, while the other two 3-phase winding sets are still operational to provide the torque. The machine specification is shown in Table I. The test rig set up is shown in Fig. 8. The machine shaft is connected to the dynamometer via an inline torque transducer. The torque of the machine is determined by the machine currents which can be controlled by the driving system consisting of three standard 3-phase inverters controlled by three DSP cores independently. The magnitude of the injected signal with respect to the modulation index is set to be 0.05, and all the signal processing is conducted in a Texas Instrument DSP controller. The implemented digital filters and RMS detectors are identical with the same gains for the three phase currents.

The severity of a turn fault is usually defined as the resultant fault current level normalized to the rated current. It is inversely proportional to the ratio of the number of short-circuited turns to the total number of the series connected turns in a phase. The lower the ratio, the larger the short-circuit current and hence the higher the severity. Also, according to [24], the 3-phase system is more unbalanced, and the conventional fault signatures such as 3rd harmonic of phase current, and 2nd harmonic of dq voltages, are higher when more turns are faulted. Therefore, the detection of one single turn short-circuit fault is essential but most challenging, and is tested in the experiments. Compared with turn fault, the effect of HRC fault is less severe, where no significantly high current may result. The HRC conditions is quantified by the increase of the phase resistance against its nominal value. The HRC fault with 0.1 Ω additional resistance is tested because it generates similar fault signatures to that of one turn fault in dq currents/voltages, negative sequence signals and PWM current ripples especially at low speed.

A single turn short-circuit fault in coil B2 of the 3-phase winding set ABC and a 0.1 Ω HRC fault in phase A are emulated by controlling a relay separately. Since the impact of the HRC faults on the conventional and the PWM ripple current based turn fault detection [17] is more significant at lower speed, where the misdiagnosis risk is higher, the

proposed turn fault detection algorithm is mainly validated below 1000 r/min.
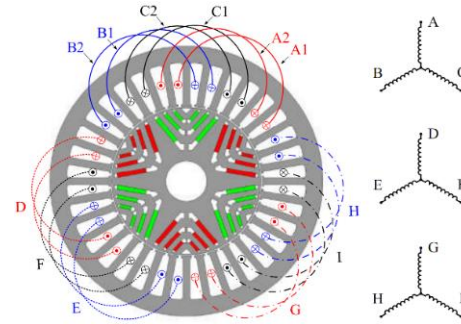

Fig. 7. Triple redundant PMA SynRM with segregated windings

TABLE I MACHINE SPECIFICATIONS

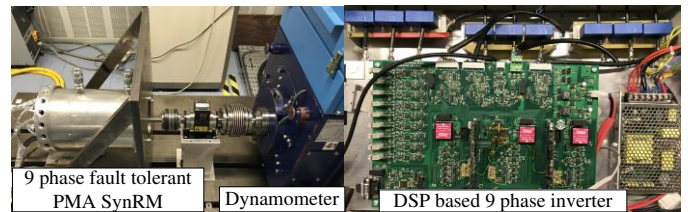| Specification	Symbol	Value
Base speed	n_b	4000 rpm
Maximum speed	n_m	19200 rpm
Rated power	P_r	35 kW
Rated current	I_{rated}	120 A peak
Nominal DC link voltage	V_{dc}	270 V
Turn number of each coil	N	8
Number of faulted turns	N_f	1
PM flux linkage	λ_{pm}	0.025 Wb
Phase resistance	R_s	0.025 Ω
d-axis inductance (nominal)	L_d	0.38 mH
q-axis inductance (nominal)	L_q	1.02 mH

Fig. 8. The 9-phase PMA SynRM test rig and DSP controlled 9-phase inverter

The machine is firstly operating at 500 r/min under the phase current of 50A with 1667Hz voltage signals injected when a single turn fault occurs at 0.11s. The responses of the relevant signals are shown in Fig. 9. The additional high frequency components can be seen in the voltages and currents. Because their amplitudes are very low, the machine operating performance is not affected in any significant manner. After the occurrence of the turn fault in phase B, 2nd harmonic appears in both dq voltages and currents, which are conventionally used for the turn fault detection. In addition, the change of the injected high frequency(HF) components can also be observed, and the increase in the current ripples of phase B is illustrated. The filtered high frequency components with BPF gains and their calculated RMS values are shown in Fig. 10. It is evident that the magnitude of the high frequency current in phase B is the largest. This is due to the reduction of the high frequency impedance in the faulted phase being the largest. To avoid the dependence of the fault detection on operating conditions, the ratios and their standard deviation among the three RMS values are calculated, to determine the

overall degree of asymmetry. The significant increase of the standard deviation can be used to detect the turn fault.
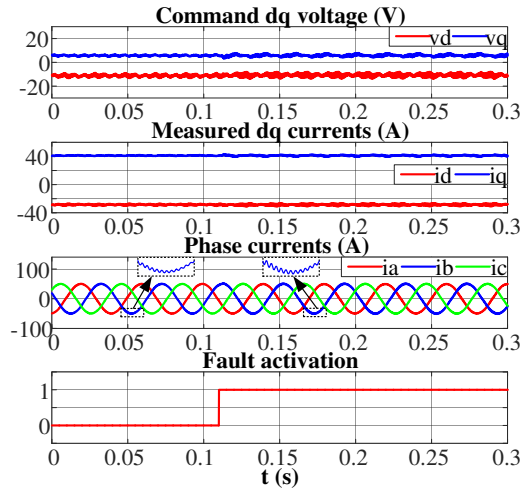

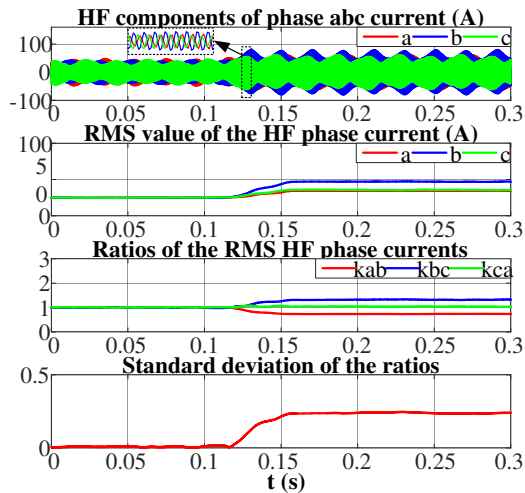Fig. 9. Dq axis voltages and phase currents at 500 r/min and 50A in healthy and turn fault conditions

Fig. 10. The high frequency currents with BPF gains, RMS detector outputs, and their ratios and standard deviation in healthy and turn fault conditions
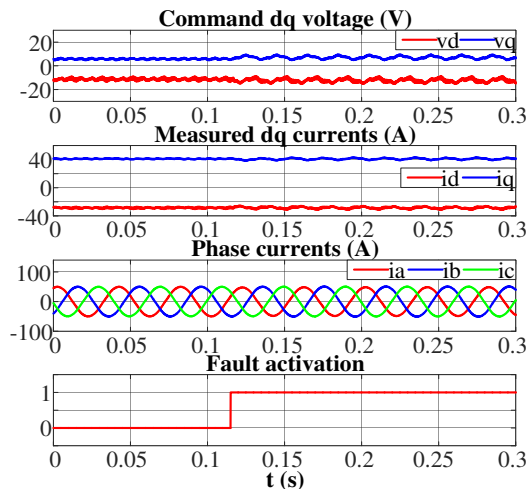

Fig. 11. Dq axis voltages and phase currents at 500 r/min 50A in healthy and HRC fault condition
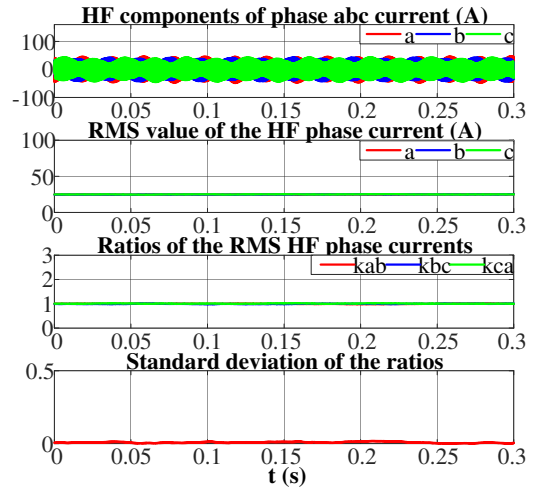

Fig. 12. The high frequency currents with BPF gains, RMS detector outputs, and their ratios and standard deviation in healthy and HRC fault conditions

When the machine is operating at the same condition and a 0.1 Ω HRC fault is activated at 0.11s, the resultant voltages and currents are shown in Fig. 11. As can be seen, the 2nd harmonic is also introduced by the HRC fault, which may trigger a false alarm of the turn fault if the conventional detection methods are used. The features in the high frequency components are shown in Fig. 12, and they are quite different from those in the turn fault condition. When the HRC fault occurs, the high frequency currents remain the same as those in the healthy condition, so do their symmetrical features. This is because the invariance of the injected voltages and the high frequency impedance. As a result, the ratios stay at 1, and the standard deviation remains at 0. Therefore, the standard deviation of the high frequency RMS current ratios is an exclusive indicator for the turn fault.

The variations of the fault indicator of the standard deviation under different operating speeds and load currents in healthy and turn fault conditions are shown in Fig. 13, which are denoted as 'H' and 'TF' respectively. The fault indicators under these two conditions differ by a large margin with great consistency independent of the operating conditions. Thus, a simple threshold can be defined to detect the turn fault exclusively. It needs to be noted the turn fault detection based on the proposed indicator can also be effective at no load (0A) conditions, because the injected signals are independent from the driving currents. As the asymmetry of the high frequency current components is used to generate the fault indicator (standard deviation of the ratios), it is determined by the effect of the turn fault on the symmetry of the machine parameters. More turns short circuit fault introduces greater asymmetry and a higher fault indicator with the same zero short circuit resistance as in the test, thus, the detectability can be improved. For turn fault with non-zero short circuit resistance, the effect on the asymmetry can be reduced, and the fault indicator is smaller. However, whether such turn fault is still detectable or not depends on the inherent symmetry of the machine in healthy conditions and the consistency of the three current transducers. In ideal conditions, the fault indicator in

healthy conditions is zero, leaving a wider applicability for different turn fault severities.
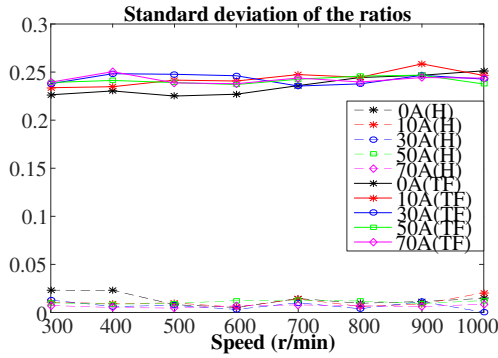

Fig. 13. Variations of fault indicators with speeds and currents in turn fault and healthy conditions

The effects of speed and current changes on the fault indicator in healthy condition are tested and illustrated in Fig. 14 and Fig. 15, where the former shows the effect with the current step change and the latter with the speed change. When the step change in current from 30A to 70A occurs at 0.2s at 500 r/min, the high frequency components increase, because the inductance decreases due to the slight increase in saturation. Since the changes in the three phase high frequency currents are not exactly synchronous, the ratios and standard deviation are slightly affected during the transient period. However, compared to the more significant increase of the indicator in the turn fault conditions in Fig. 10, such disturbance caused by the transient will not trigger a false alarm if a proper threshold is determined. When the speed increases linearly with the acceleration of 1000 (r/min)/s in the healthy condition in Fig. 15, the results are not affected at all. A good isolation of the injected frequency signals from the fundamental signals guarantees that the fault indicator is immune to the transient states, avoiding any risk of false alarms. When the turn fault occurs at the same time when the operating condition changes as shown in Fig. 16 and Fig. 17, the fault detection is still effective. Thus, the reliability and robustness of the proposed fault indicator with the high frequency voltage injection for detecting the turn fault have been demonstrated.

VII. DISCUSSIONS

The key challenge addressed in this paper is the ambiguity in identifying two fault types: turn fault and an HRC fault, which results with detection techniques reported in literature when the machine operates at low speed. Incorrect identification or false alarm would result in a serious consequence. For example, if a turn fault is misdiagnosed as an HRC fault with no immediate action taken, the fault would quickly lead to complete failure and loss of the entire drive system with catastrophic consequence in safety critical applications. Conversely, if an HRC faults is wrongly identified as a turn fault, a mitigation action, typically application of terminal short-circuit via the 3-phase inverter, would lead to unnecessary reduction of torque capability. It

has been demonstrated that this problem has been effectively resolved with the proposed technique.

While the focus of the proposed technique is on exclusive detection of a turn fault, its combination with the techniques reported in literature can be used to detect an HRC fault when the 2nd harmonic in the dq voltages or currents is detected while a turn fault is ruled out by the proposed detection technique.

Compared with the conventional turn fault detection technique using high frequency signal injection in [18], the newly proposed method does not use coordinate transformation, but compare the high frequency signatures among three phases, which makes it more robust to transient states. Specific square-wave signals whose frequency are fixed as 1/6 of the switching frequency are injected, thus enlarging the applicable speed range compared with the conventional sinusoidal signal injection based methods

The fault indicator proposed in this paper is calculated from the ratios of the three phase high frequency current components. Since the effect of transient states on the high frequency currents are almost the same, and the RMS values of the filtered signals change simultaneously, such effect on the ratios has been largely minimized. The effects of different speeds or loads conditions on the high frequency currents of three phases can be slightly different but much closer, compared to those of turn fault conditions. Also, with the measurement errors present, the final calculated fault indicator shows good consistency within a relatively small margin. Therefore, a great robustness towards transient and load and speed variations can be achieved.
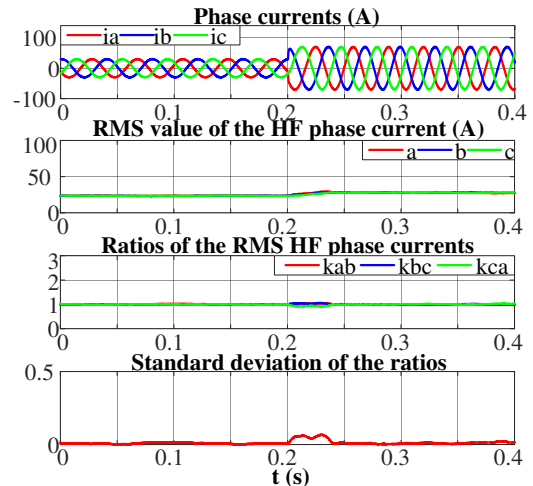

Fig. 14. Healthy condition with current step change (a) speed, dq axis voltages and phase currents, (b) the high frequency currents, RMS detector outputs, and their ratios and standard deviation

The injection of the high frequency signal would cause extra torque ripple and loss in the drive system. However, injection is only necessary when the speed is below ~25% of the base speed and the 2nd harmonic has been detected. The typical detection response time of the two detection process under this condition is below 100ms in which the temperature increase with the one turn short-circuit fault would not lead to

irreversible damage due to relatively large thermal time constant of the machine winding [25].
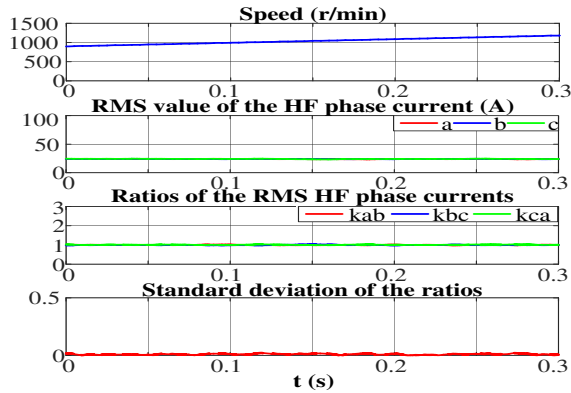

Fig. 15. Healthy condition with increasing speed (a) speed, dq axis voltages and phase currents, (b) the high frequency currents, RMS detector outputs, and their ratios and standard deviation
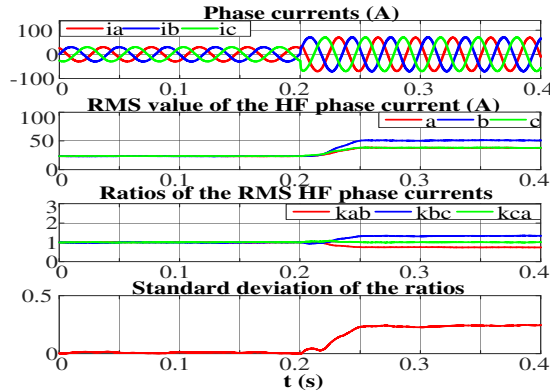

Fig. 16. Turn fault condition with current step change (a) speed, dq axis voltages and phase currents, (b) the high frequency currents, RMS detector outputs, and their ratios and standard deviation
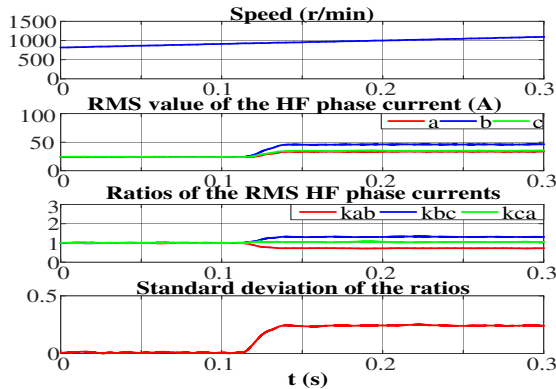

Fig. 17. Turn fault condition with increasing speed (a) speed, dq axis voltages and phase currents, (b) the high frequency currents, RMS detector outputs, and their ratios and standard deviation

It should also be noted that ambiguity of an HRC fault and a turn-fault is most pronounced when a turn fault involves in only one short-circuit (SC) turn while the machine operates at low speeds. This is because the asymmetry with more SC turns or at high speed is much greater and can be much easily detected. Thus, the experimental results presented in the paper

have already covered the worst case for validation of the proposed technique.

VIII. CONCLUSIONS

This paper proposes a high frequency voltage injection based turn fault detection with the discrimination from an HRC fault. The high frequency voltages of the square wave are injected into the modulating signals of the space vector PWM control at 1667 Hz. The symmetry of the corresponding high frequency currents is examined, based on which a new turn fault indicator is proposed. The theoretical analysis and experiments have demonstrated the exclusivity for the detection of turn fault. The fault indicator is insensitive to operating conditions due to its isolation from the fundamental components and this makes it easier to determine the threshold to separate the fault from health conditions. The robustness of the detection to the transient states is also verified. The required 10 kHz sampling and data processing can be implemented in the DSP controller to extract the high frequency components and calculate the RMS values digitally with no additional hardware needed. Thus, this turn fault method can be conveniently implemented when necessary.

REFERENCES

[1] IEEE, "Motor Reliability Working Group, Report of Large Motor Reliability Survey of Industrial and Commercial Installations," *IEEE Trans. Ind. Appl.*, vol. IA-4, July, no. 4, pp. 853–872, 1985.

[2] S. Grubic, J. M. Aller, B. Lu, and T. G. Habetler, "A survey on testing and monitoring methods for stator insulation systems of low-voltage induction machines focusing on turn insulation problems," *IEEE Trans. Ind. Electron.*, vol. 55, no. 12, pp. 4127–4136, 2008.

[3] A. Gandhi, T. Corrigan, and L. Parsa, "Recent advances in modeling and online detection of stator interturn faults in electrical motors," *IEEE Trans. Ind. Electron.*, vol. 58, no. 5, pp. 1564–1575, 2011.

[4] K.-H. Kim, D.-U. Choi, B.-G. Gu, and I.-S. Jung, "Online fault-detecting scheme of an inverter-fed permanent magnet synchronous motor under stator winding shorted turn and inverter switch open," *IET Electr. Power Appl.*, vol. 5, no. 6, pp. 529–539, 2011.

[5] Y. Mollet, X. Kestelyn, F. Meinguet, E. Semail, and J. Gyselinck, "Change-detection algorithm for short-circuit fault detection in closed-loop AC drives," *IET Electr. Power Appl.*, vol. 8, no. 5, pp. 165–177, 2014.

[6] B. Wang, J. Wang, A. Griffo, and B. Sen, "Stator Turn Fault Detection by Second Harmonic in Instantaneous Power for a Triple-Redundant Fault-Tolerant PM Drive," *IEEE Trans. Ind. Electron.*, vol. 65, no. 9, pp. 7279–7289, 2018.

[7] S. M. A. Cruz and A. J. Marques Cardoso, "Stator winding fault diagnosis in three-phase synchronous and asynchronous motors, by the extended park's vector approach," *IEEE Trans. Ind. Appl.*, vol. 37, no. 5, pp. 1227–1233, 2001.

[8] H. Jeong, S. Moon, and S. W. Kim, "An Early Stage Interturn Fault Diagnosis of PMSMs by Using Negative-Sequence Components," *IEEE Trans. Ind. Electron.*, vol. 64, no. 7, pp. 5701–5708, 2017.

[9] R. M. Tallam, T. G. Habetler, and R. G. Harley, "Stator winding turn-fault detection for closed-loop induction motor drives," *IEEE Trans. Ind. Appl.*, vol. 39, no. 3, pp. 720–724, 2003.

[10] J. C. Urresty, J. R. Riba, and L. Romeral, "Diagnosis of interturn faults in pmsms operating under nonstationary conditions by applying order tracking filtering," *IEEE Trans. Power Electron.*, vol. 28, no. 1, pp. 507–515, 2013.

[11] J. Hang, J. Zhang, M. Cheng, B. Zhang, and S. Ding, "High-Resistance Connection Detection in Permanent Magnet Synchronous Machine Using Zero-Sequence Current Component," *IEEE Trans. Power Electron.*, vol. 31, no. 7, pp. 4710–4719, 2016.

[12] R. D. Naybour and T. Farrell, "Degradation mechanisms of mechanical connectors on aluminium conductors," *Proc. Inst.*

Electr. Eng., vol. 120, no. 2, pp. 273–280, 1973.

[13] M. Braunovic, "Effect of Connection Design on the Contact Resistance of High Power Overlapping Bolted Joints," *IEEE Trans. Components Packag. Technol.*, vol. 25, no. 4, pp. 642–650, 2002.

[14] J. Yun, J. Cho, S. Bin Lee, and J. Y. Yoo, "Online detection of high-resistance connections in the incoming electrical circuit for induction motors," *IEEE Trans. Ind. Appl.*, vol. 45, no. 2, pp. 694–702, 2009.

[15] J. Yun, K. Lee, K. W. Lee, S. Bin Lee, and J. Y. Yoo, "Detection and classification of stator turn faults and high-resistance electrical connections for induction machines," *IEEE Trans. Ind. Appl.*, vol. 45, no. 2, pp. 666–675, 2009.

[16] B. Sen, "Modelling , Fault Detection and Control of Fault Tolerant Permanent Magnet Machine Drives," *PhD Thesis, University of Sheffield, UK, September*, 2015.

[17] R. Hu, J. Wang, A. R. Mills, E. Chong, and Z. Sun, "PWM Ripple Currents Based Turn Fault Detection for 3-phase Permanent Magnet Machines," *IEEE Int. Electr. Mach. Drives Conf.*, pp. 1–7, 2017.

[18] F. Briz, M. W. Degner, A. Zamarron, and J. M. Guerrero, "On-line stator winding fault diagnosis in inverter-fed ac machines using high frequency signal injection," *IEEE Trans. Ind. Appl.*, vol. 39, no. 4, pp. 1109–1117, 2003.

[19] R. Hu, J. Wang, A. R. Mills, and E. Chong, "Detection and Classification of Turn Fault and High Resistance Connection Fault in Permanent Magnet Machines based on Zero Sequence voltage," *IEEE Trans. Power Electron.*, *Early Access*, 2019.

[20] B. Vaseghi, B. Nahid-Mobarakh, N. Takorabet, and F. Meibody-Tabar, "Inductance identification and study of PM motor with winding turn short circuit fault," *IEEE Trans. Magn.*, vol. 47, no. 5, pp. 978–981, 2011.

[21] Y. Qi, E. Bostanci, V. Gurusamy, and B. Akin, "A Comprehensive Analysis of Short Circuit Current Behavior in PMSM Inter Turn Short Circuit Faults," *IEEE Trans. Power Electron.*, vol. 33, no. 12, pp. 10784–10793, 2018.

[22] R. Hu, J. Wang, B. Sen, A. R. Mills, E. Chong, and Z. Sun, "PWM Ripple Currents Based Turn Fault Detection for Multiphase Permanent Magnet Machines," *IEEE Trans. Ind. Appl.*, vol. 53, no. 3, pp. 2740–2751, 2017.

[23] B. Wang, J. Wang, B. Sen, A. Griffo, Z. Sun, and E. Chong, "A Fault-Tolerant Machine Drive Based on Permanent Magnet-Assisted Synchronous Reluctance Machine," *IEEE Trans. Ind. Appl.*, vol. 54, no. 2, pp. 1349–1359, 2018.

[24] M. Zafarani, S. Member, E. Bostanci, Y. Qi, and S. Member, "Inter-turn Short Circuit Faults in Permanent Magnet Synchronous Machines : An Extended Review and Comprehensive Analysis," *IEEE J. Emerg. Sel. Top. Power Electron.*, vol. 6, no. 4, pp. 2173–2191, 2018.

[25] Y. Shi, J. Wang, and B. Wang, "EM-thermal coupled simulation under various fault conditions of a triple redundant 9-phase PMASynRM," in *Proc. 2018 IEEE Energy Convers. Congr. Expo.*, pp. 5757–5764, 2018.